

# FINE STRUCTURE IN SOME LANDSCAPES OF L-FUNCTIONS

DAVID W. FARMER, SALLY KOUTSOLIOTAS, STEFAN LEMURELL,  
AND DAVID P. ROBERTS

ABSTRACT. We present three examples in an emerging theory of fine structure in landscapes of L-functions. These examples illustrate how the classical principles of zero repulsion and zero rigidity underlie the novel phenomena of ditch avoidance and congruence bias.

In our LuCaNT 2023 paper [3] we organized collections of L-functions by representing each L-function as an “L-point” in a Euclidean region, thereby obtaining what we call landscapes. The last paragraph in [3, §3.1] asked for an explanation of a striation phenomenon very visible in the landscape presented as [3, Figure 3.1]. The report [8] continued the study of this particular landscape, emphasizing certain *fine structure* that underlies the striation phenomenon. It also sketched how we expect such fine structure to be present in general landscapes. This theory is still mainly in an experimental stage, and it is important to have data from as many landscapes as possible so as to, for example, understand how the strength of fine structure varies in different regimes.

Sections 1, 2, and 3 draw increasingly complex landscapes and explain with reference to these examples what we mean by fine structure. Section 4 uses zeros of the L-functions in question to heuristically explain striations in terms of *ditch avoidance*. Section 5 explains how the nature of the ditches causes a *congruence bias* that we did not even suspect when we wrote [3]. Section 6 was added in the revision stage of this paper; it uses the newly found [6] as an essential starting point, and takes next steps towards making the theory rigorous. Because of the examples-first structure of this paper, some readers may want to take an early look at the later more general sections. For example, understanding trapped zeros as illustrated by Figure 4 facilitates the reading of the first three sections.

We follow the general conventions of [3]. Our analysis uses only the functional equation, which we write in the form

$$\Lambda_L(s) := G_L(s)L(s) = \varepsilon_L \overline{\Lambda}_L(1-s)$$

where  $\overline{f}(z) := \overline{f(\overline{z})}$ . We refer to  $G_L(s)$  as “the  $\Gamma$ -factors,” but it also contains a factor  $N^{s/2}$  where  $N$  is the conductor of the L-function. We refer to  $\varepsilon_L$  as “the sign,” and it is a complex number on the unit circle. Central to our theory is that the  $\Gamma$ -factors and the sign of a given L-function give a “best first guess” at where the critical zeros of the L-function are. These best first guesses involve the Riemann-Siegel theta function and close analogs, and are slightly too complicated to describe here.

The degree 2 data we use come from numerical computations of [9], with initial segments of the data being made completely rigorous in the LMFDB [7]. Our degree 3 data were generated using “L-functions out of nothing” [2, 5] and are thus heuristic; data are available at [4].

## 1. FIXED SIGN, ONE SPECTRAL PARAMETER

The two simplest nontrivial landscapes come from Maass forms on  $\mathrm{SL}(2, \mathbb{Z})$ . The corresponding degree 2 L-functions have  $G_L(s) = \Gamma_{\mathbb{R}}(s + \delta + i\lambda)\Gamma_{\mathbb{R}}(s + \delta - i\lambda)$ , where  $(\delta, \varepsilon_L) = (0, 1)$  for even Maass forms, and  $(1, -1)$  for odd Maass forms. The landscapes are drawn in Figure 1, with ditches represented by vertical segments. They occur where the best first guess places a zero at  $\frac{1}{2} + \lambda i$ , in which case it also places a zero at  $\frac{1}{2} - \lambda i$ . The ditches occur at the local minima of  $w_{\pm}(t) = \cos\left(2t \log\left(\frac{t}{e\pi}\right) \mp \frac{\pi}{4}\right)$ , where + and - on the left indicate the even and odd cases.

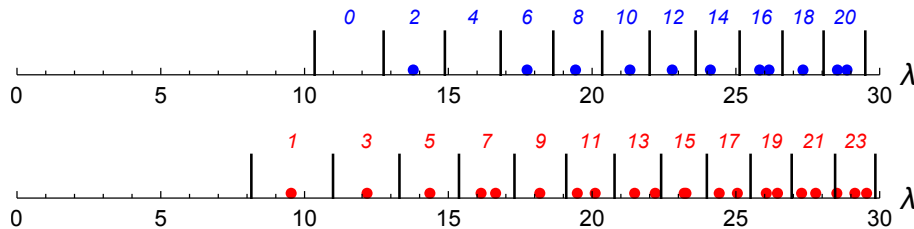


FIGURE 1. L-points of even (top) and odd (bottom) Maass forms on  $\mathrm{SL}(2, \mathbb{Z})$ .

A key role in our theory in this instance is the number  $z_1$  of **trapped zeros** of a given L-function. A zero is trapped when its imaginary part is in  $(-\lambda, \lambda)$ . An interval between adjacent ditches is labeled by the expected number of trapped zeros for any L-points in it. A key point is that this number, as well as its analogs in later sections, is computable, like the ditches are, from  $G_L(s)$  and  $\varepsilon_L$  only.

One can see that there is a tendency of L-points to avoid ditches, and that this tendency is stronger in the even case. Not evident from the picture is that, for all the drawn L-points, the number of trapped zeros agrees with the expected number of trapped zeros. The ditch avoidance, and the matching of actual and expected numbers of trapped zeros, are aspects of fine structure.

A more analytic way to capture ditch avoidance is to consider the sum  $f_{\varepsilon}(T) = \sum_{\lambda < T}^{\varepsilon} w_{\varepsilon}(\lambda)$ , with the superscript on the sum indicating that only  $\lambda$  of parity  $\varepsilon$  are included. If there were no ditch avoidance phenomenon, since  $w_{\varepsilon}$  is 0 on average one would expect  $f_{\varepsilon}(T)$  to remain very small as the cutoff  $T$  increases, and moreover exhibit chaotic oscillations. However, the observed behavior is very different as follows. In the interval  $[0, 1400]$  the data from [9] says that there are 77926 and 80044 different  $\lambda$  coming from even and odd Maass forms respectively. One has  $f_{+}(1400) = 6250.1$  and  $f_{-}(1400) \approx 236.1$ . The numerical fits  $f_{+}(T) \approx 0.111 T^{1.509}$  and  $f_{-}(T) \approx 3.433 T^{0.582}$  are quite accurate over the entire interval  $[0, 1400]$ . Thus ditch avoidance persists well past the window of Figure 1, being strong in the even case and much weaker in the odd case. This purely experimental finding on  $f_{+}(T)$  will be improved in Section 6, while the experimental finding on  $f_{-}(T)$  is too subtle for current theory.

## 2. VARYING SIGN, ONE SPECTRAL PARAMETER

Our next example concerns L-functions of degree 3 and conductor 4. If the local representation at 2 is Steinberg, then the sign is a cube root of 1, and otherwise the sign is not restricted. In Figure 2 we combine both cases, with the argument of the sign on the vertical axis, and the spectral parameter  $\lambda$  on the horizontal axis. We

could draw the ditches sharply, like we did in Figure 1 of [8]. However we present them instead as they were first encountered in our numerical explorations.

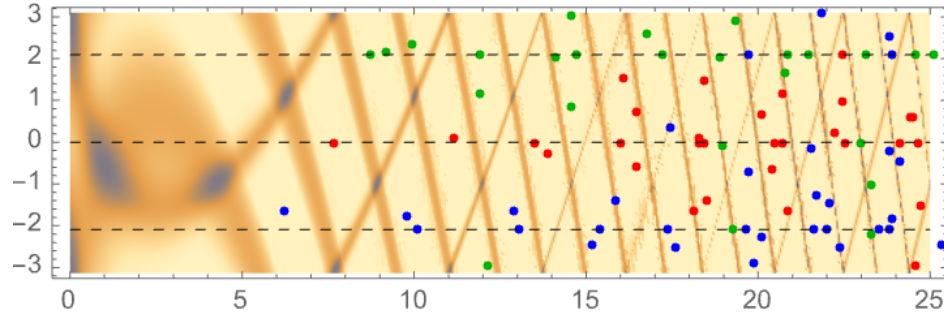


FIGURE 2. L-points with  $\Gamma$ -factor  $G_L = 4^{s/2}\Gamma_{\mathbb{R}}(s+i\lambda)\Gamma_{\mathbb{C}}(s+\frac{3}{2}-i\lambda/2)$ .

An upward ditch occurs when the best first guess places a zero at  $\frac{1}{2} - \lambda i$  while a downward ditch occurs when it places a zero at  $\frac{1}{2} + \frac{\lambda}{2}i$ . The L-points have a strong tendency to avoid the former and a weaker tendency to avoid the latter. Here a zero is trapped if its imaginary part is in  $(-\lambda, \frac{\lambda}{2})$ . As before, the numbers indicate the expected number of trapped zeros. Here, the actual number  $z_1$  of trapped zeros is within one of the expected number. To make the actual number readable on the picture, we color points blue, red, or green according to whether  $z_1$  is 0, 1, or 2 modulo 3. So L-points are mostly in their correct regions, the first deviation being that the green L-point in the blue region 3 actually has only 2 trapped zeros.

### 3. TWO SPECTRAL PARAMETERS

Our final example revisits Figure 3.2 of [3], but now with superimposed ditches and L-point coloring. Striations were clearly visible before, but are now explained by ditches which go between them.

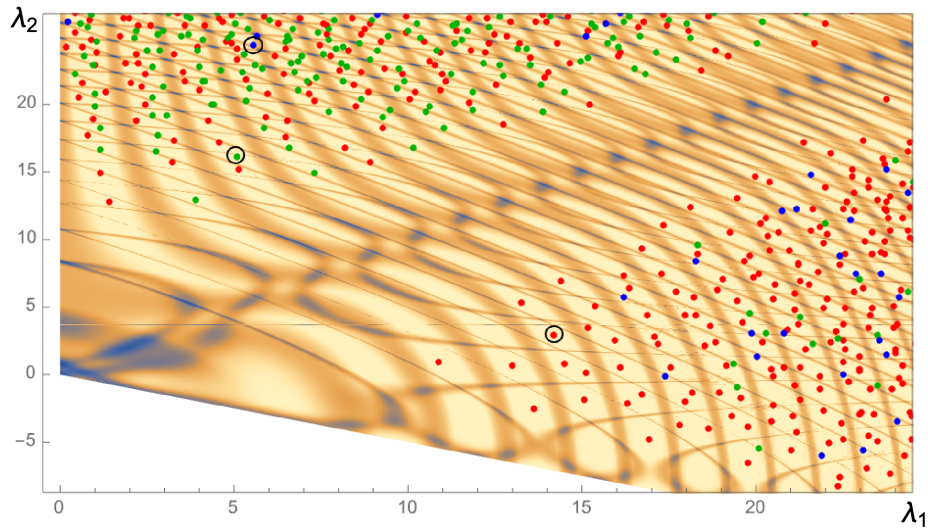


FIGURE 3. L-points with  $G_L(s) = \Gamma_{\mathbb{R}}(s+i\lambda_1)\Gamma_{\mathbb{R}}(s+1+i\lambda_2)\Gamma_{\mathbb{R}}(s+1+i\lambda_3)$

As illustrated in Figure 4 below, each L-function has an associated vector  $(z_1, z_2)$ , where  $z_j$  is the number of critical zeros with imaginary part in  $(\lambda_j, \lambda_{j+1})$ . Each region also has such an integral vector, the expected vector of trapped zeros for L-points in that region. From the general recipe from [8], it is good to focus on the difference  $c = z_2 - z_1$  in  $\mathbb{Z}/3$ . L-points are colored blue, red, or green, according to their class  $c$ . About 80% of the L-points are in their correct region, so that one can infer the color of regions from the figure. In the upper regime, area is divided evenly between red = 1 and green = 2, with no area allocated to blue = 0. In the lower regime, each  $c$  occurs, with red = 1 occurring in hexagons, and the remaining classes occurring only in small triangles, which are six times smaller.

#### 4. ZERO REPULSION AND ZERO RIGIDITY FORCE DITCH AVOIDANCE

Here we explain the section title via our third example, the other two examples being similar but easier. The three plots in Figure 4 show the trivial and critical zeros of the circled L-points in Figure 3, in order of increasing horizontal coordinate. Note that there is an evident *zero repulsion* between the trivial zeros and critical zeros, and the effect is greater when the trivial zeros are closer to the critical line.

The best guess at zeros is indicated by horizontal segments. They come from the first term of the Riemann-Siegel formula, which depends only on  $G_L(s)$  and  $\varepsilon_L$ . The fact that the actual zeros do not stray too far from their predicted locations is *zero rigidity*. One can see rigidity in the case of the  $\zeta$ -function by executing `Plot[{RiemannSiegelZ[t], 2 Cos[RiemannSiegelTheta[t]]}, {t, 0, 100}]` in *Mathematica* or on `wolframalpha.com`.

Recall that the ditches occur where a predicted zero agrees with a row of trivial zeros. Zero repulsion says that there should not be an actual zero nearby. Zero rigidity says that there should be an actual zero nearby. We resolve this contradiction by a *ditch avoidance* principle that says that L-points are less likely to occur near ditches.

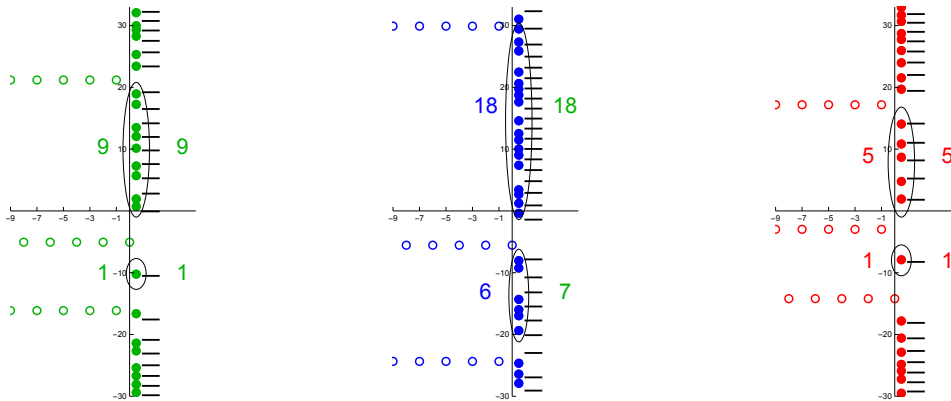


FIGURE 4. The zeros of the three circled L-functions in Figure 3

Zero repulsion and zero rigidity together make the actual number of zeros likely to be close to the predicted number of zeros. Deviations from prediction can be expected to be greater as conductors or spectral parameters increase. In Figure 4, the prediction is correct for the outer two L-functions. However, the blue L-point

indexing the inner L-function is in a triangle in Figure 3 corresponding to the color green. For L-points in this triangle, the prediction is (7, 18). This particular L-function with its actual  $(z_1, z_2) = (6, 18)$  is off by one.

### 5. REGION SIZES CAUSE CONGRUENCE BIAS

The outline in [8] says that for degree  $d$  L-functions, both regions and L-points have a class in  $\mathbb{Z}/d\mathbb{Z}$ . For fixed  $\varepsilon$ , the probability measure on  $\mathbb{Z}/d\mathbb{Z}$  induced by the region sizes can be calculated and it differs markedly from the uniform distribution. This deviance was already discussed in the last paragraph of Section 3, where classes 0, 1, 2 have an area split of  $(0, 1/2, 1/2)$  and  $(1/8, 3/4, 1/8)$  in the upper and lower regions respectively. To the extent that L-points tend to be in their correct region, their class coming from the configuration of trapped zeros would be biased too.

In our three examples, congruence bias looks as follows. For Figure 1, on each line only one parity occurs for  $z_1$ . One can say that the extreme congruence bias is enforced by the parity of the L-function. In Figure 2, each dashed line is 50% in its dominant color and 25% in the other colors. But the L-points are almost entirely in the dominant color. In Figure 3, the L-point bias is moderately close to the region bias, in both the upper and lower regimes.

### 6. TOWARDS A RIGOROUS THEORY OF FINE STRUCTURE

While revising this paper, we found a paper by C. J. Mozzochi [6]. Mozzochi works with  $w_q(t) = \cos(2t \log(\frac{qt}{e\pi}) - \frac{\pi}{4})$ , where  $q > 0$  is a parameter. Summing over  $\lambda$  of both parities, he remarks that, translating to our style of cutoffs, the “trivial bound” for  $\sum_{\lambda < T} w_q(\lambda)$  from the Selberg trace formula is  $O(T^{3/2})$ . His Theorem 1 then says that for  $q$  the reciprocal of an integer, the exponent  $3/2$  cannot be lowered. Thus, taking  $q = 1$ , [6] is proving the indefinite continuation of ditch avoidance in the classical context of  $SL_2(\mathbb{Z})$ , already in 1999! It is moreover proving that the  $\lambda$  also avoid other collections of ditches, one for each reciprocal integer.

We are in the process of generalizing and sharpening Mozzochi’s theorem to

$$\sum_{\lambda < T}^{\varepsilon} w_q(\lambda) = \frac{a_q^{\varepsilon} T^{3/2}}{3\pi^{3/2}} + o(T^{3/2}),$$

with the expectation that we can obtain power-saving error term. Thus we are refining by fixing the parity  $\varepsilon$  and giving a specific growth constant. The factor  $a_q^{\varepsilon}$  is 0 if  $q$  is irrational and is given by a complicated explicit formula if  $q$  is rational. For  $q = 1, 2, 3, 4$  our formula gives  $a_q^+ = 2, 4/3, 3/8, 0$  and  $a_q^- = 0, 0, -9/8, -4/3$ . As two examples, least square fits as in §1 except with the exponent fixed at  $3/2$  give  $\sum_{\lambda < T}^+ w_1(\lambda) \approx 2 \cdot 0.05966 T^{3/2}$  and  $\sum_{\lambda < T}^- w_4(\lambda) \approx -4/3 \cdot 0.05984 T^{3/2}$ . These numerics compare well with  $1/(3\pi^{3/2}) \approx 0.05986$ .

We expect this approach will give similar results for ditch avoidance of  $\lambda$  coming from classical Maass forms of any level and character. A promising future direction is to see what the Selberg trace formula gives for larger groups, such as congruence subgroups of  $SL_3(\mathbb{Z})$  as in §2 and §3. Note that the explanation of ditch avoidance via the Selberg trace formula does not make direct reference to L-functions or their zeros! Thus one is still in search of an appropriate tool for rigorously understanding congruence bias.

## REFERENCES

- [1] Farmer, David W., Currently there are no reasons to doubt the Riemann Hypothesis: the zeta function beyond the realm of computation. preprint. <https://arxiv.org/abs/2211.11671>.
- [2] Farmer, David W.; Koutsoliotas, Sally; Lemurell, Stefan, Maass forms on  $GL(3)$  and  $GL(4)$ . *Int. Math. Res. Not. IMRN* 2014, no. 22, 6276-6301.
- [3] Farmer, David W.; Koutsoliotas, Sally; Lemurell, Stefan; Roberts, David P., The landscape of L-functions: degree 3 and conductor 1. *LuCaNT: LMFDB, computation, and number theory*, 313–338. *Contemp. Math.*, 796 American Mathematical Society, 2024.
- [4] <https://github.com/davidfarmer/LandscapeData>
- [5] <https://github.com/lemurell/Euler/>
- [6] Mozzochi, C. J. On the distribution of the eigenvalues of the hyperbolic Laplacian for  $PSL(2, \mathbb{Z})$ . *II. J. Number Theory* 86 (2001), no. 2, 284?301.
- [7] The LMFDB Collaboration, The L-functions and modular forms database, <https://www.lmfdb.org/ModularForm/GL2/Q/Maass/>, 2025.
- [8] Roberts, David P., Landscapes of L-functions, Oberwolfach Workshop 2436, report 40/2024, <https://publications.mfo.de/handle/mfo/4254>, p. 26-28.
- [9] Then, Holger, Maass cusp forms for large eigenvalues, *Math. Comp.* 74 (2005) 363-381

AMERICAN INSTITUTE OF MATHEMATICS

*Email address:* [farmer@aimath.org](mailto:farmer@aimath.org)

BUCKNELL UNIVERSITY

*Email address:* [koutslts@bucknell.edu](mailto:koutslts@bucknell.edu)

CHALMERS UNIVERSITY OF TECHNOLOGY AND UNIVERSITY OF GOTHENBURG

*Email address:* [sj@chalmers.se](mailto:sj@chalmers.se)

UNIVERSITY OF MINNESOTA MORRIS

*Email address:* [roberts@morris.umn.edu](mailto:roberts@morris.umn.edu)